ARMA 20–1982

SAND2020-2878C

Characterization of Permeability/Porosity Relationships as a Function of Rubble Pile Polydispersity during Room Closure at the Waste Isolation Pilot Plant

Matteo, E. N., Mitchell, C., and Dewers, T. A.
Sandia National Laboratories, Albuquerque, NM, USA

Lander, R. and Bonnell, L.
Geocosm, LLC, Durango, CO, USA

ABSTRACT: Room closure is an important aspect of the safety concept and waste isolation strategy at the Waste Isolation Pilot Plant, located in southeastern New Mexico, USA. Isolation of waste constituents is achieved as disposal rooms converge upon the waste packages, and over long timescales, entomb the waste packages in an extremely low permeability mass of reconsolidated salt. If roof fall occurs, the safety case needs to take into account the evolution of permeability within the disposal room over time. This would include predictions for permeability/transport at relatively early times when the rubble pile will contain an extremely poorly-sorted mixture of large, meter-scale evaporite fragments and much smaller-sized fragments of salt at the millimeter scale.

Roof collapse at WIPP is also of interest in that resulting rubble piles likely consolidate in a manner differently from typical experimental salt consolidation tests. As a result, fluid transport during room consolidation under roof collapse scenarios has not been well characterized. Here we discuss progress toward characterizing initial rubble piles using micro-computerized tomography and computational fluid dynamics modeling of fluid transport in pore spaces within rubble. We detail methods used to separate segmented binary (solid and fluid) images and determine preliminary particle size distributions of rubble piles using image analysis software. In an initial trial, we show how particle separates are applied in a numerical scheme for particle consolidation. We use image analysis methods to extract a finite element mesh for the pore spaces within initial fractures from the disturbed rock zone and run-of-mine salt and perform example computational fluid dynamics (CFD) simulations of gas transport within representative sub-samples. We discuss paths forward in developing a methodology for modeling empty room rubble pile consolidation and gas transport at WIPP.

1. INTRODUCTION

Roof collapse at WIPP (Figure 1) is of interest in that the resulting rubble piles likely consolidate in a manner differently from typical experimental salt consolidation tests, and the resulting flow pathwayswithin the consolidation rubble have not been characterized, particularly in how these are influenced by consolidation. Here we discuss initial progress toward characterizing initial rubble piles using micro-computerized tomography and computational fluid dynamics modeling of gas transport in pore spaces within rubble. We detail methods used to separate segmented binary (solid and fluid) images and determine preliminary particle size distributions of rubble piles using image analysis software. In an initial trial, we show how particle separates are applied in a numerical scheme for particle consolidation.

Figure 1. Roof collapse and resulting rubble pile in ES300-S3650 access drift at WIPP (from Carrasco 2019).

Sandia National Laboratories is a multimission laboratory managed and operated by National Technology & Engineering Solutions of Sandia, LLC, a wholly owned subsidiary of Honeywell International Inc., for the U.S. Department of Energy's National Nuclear Security Administration under contract DE-NA0003525.

We use image analysis methods to extract a finite element mesh for the pore spaces within initial fractures from the disturbed rock zone and run-of-mine salt and perform example computational fluid dynamics (CFD) simulations of gas transport within representative sub-samples. We discuss paths forward in developing a methodology for modeling empty room rubble pile consolidation and gas transport at WIPP.

2. MATERIALS

2.1. WIPP Salt Sample Collection

Two samples of WIPP salt were collected from for our initial analysis. These are:

1. WIPP Run-of-mine salt collected from the floor of and stored in a sealed 10-gallon plastic bucket.
2. A piece of 12" drill core from the disturbed rock zone from E-140.

3. METHODS

3.1. Computerized Tomography and Image Analysis

X-ray micro-computed tomography (X-ray μCT) imaging was performed on salt samples using a North Star Imaging X50 micro-CT scanner and a Perkin Elmer 0822 1622 Digital Image detector, with North Star efX-DR and efX-CT software used for image acquisition and reconstruction, respectively, by Carl Jacques of Sandia's Nondestructive Environments and Diagnostics Department. Tomographic reconstructions were provided in the form of TIFF image stacks with a voxel size of 8.3e5 μm^3 (94 μm ×94 μm × 94 μm). We applied a variety of filters to improve the quality of salt-pore space contrast, including a median filter and edge-preserving smoothing. A segmentation algorithm was then applied to determine, label, and measure particle sizes and shapes of salt particles in the run-of-mine salt, and a particle size distribution was prepared using Excel. The Scan-IP and Scan-FE modules of the Synapsis™ software suite, Simpleware™, to visualize connected and unconnected portions of pore networks delineated by the □CT reconstructions and to prepare surface meshes of grain separates, and finite element meshes for the CFD simulations.

3.2. Geocosm Cyberstone Modeling

Cyberstone™ is Geocosm's 3D proprietary simulator used by the company in-house (patents pending) to model sedimentation, compaction, and other processes (https://geocosm.net/products/).

3.3. CFD Modeling of Gas Transport

Example CFD modeling was performed using COMSOL Multiphysics™ software, using meshes prepared from the Scan-IP software. We used densities and dynamic viscosities of dry air, and modeled the gas transport using steady-state Navier-Stokes equations keeping inertial terms and using a downstream boundary condition at one end of the domain at a constant pressure of 1 atm and an upstream constant flux of 1.0e-4 m/s.

3.4. "Drop" Test

The DRZ core piece was initially scanned, and then dropped from a height of 12 feet onto a concrete surface while contained inside a cloth bag (used to contain the fragments). The resulting pieces were placed in a plastic 10-gallon bucket and re-scanned.

4. RESULTS

4.1. Core of disturbed rock zone

Figure 2 shows 2-D radiographs and a 3D reconstruction of the DRZ core piece. In Figure 2A (scale bar is 30 mm), numerous extension fractures oriented parallel to the wall increase in density as the wall is

.

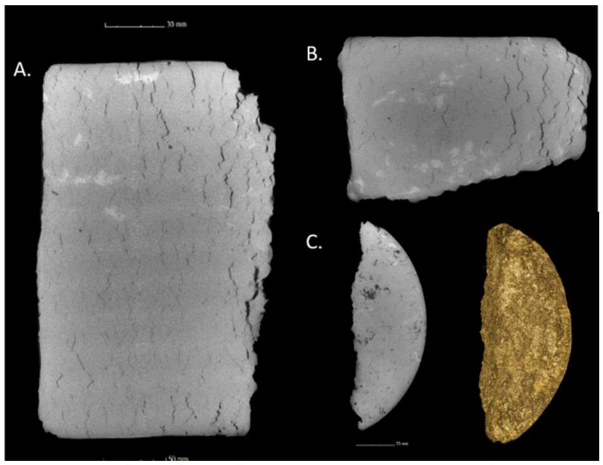

Figure 2. X-ray imaging of WIPP DRZ core sample

approached (In Figure 2A and 2B, this is the right-hand vertical boundary of the images). The fractures appear black against the grey levels of the salt and other minerals, where salt is the darkest grey, and other evaporite minerals appear as lighter shades.

4.2 Sample of run of mine salt

The run-of-mine salt sample with included bucket is shown in Figure 3. One can see just from looking at the top of the tomogram that there is a mixture of poorly sorted particles, with numerous flat pancake-like shapes for the larger grains, and more equant grains among the smaller in the distribution. A cross section view of the salt bucket is shown in Figure 4.

Figure 3. X-ray tomographic reconstruction of bucket of run-of-mine salt. The bucket is approximately 12” across.

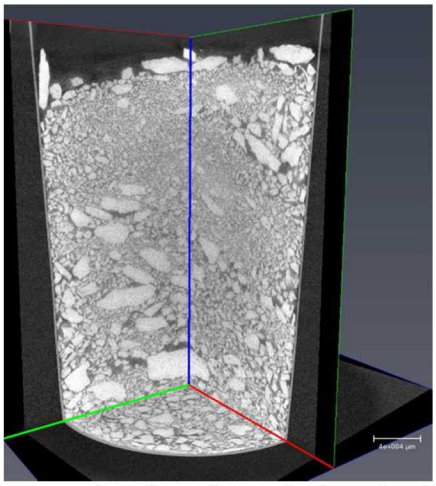

Figure 4. Cross section view of run-of-mine salt with voxel size of 94 microns.

4.3. DRZ Core from "dropped" experiment

The DRZ core piece subject to dropping is shown via tomographic reconstruction is shown in Figure 5. The piece has broken into three large pieces and many smaller pieces. Unexpectedly, many of the extension fractures visible in the unbroken piece (Figure 2) survived the fall.

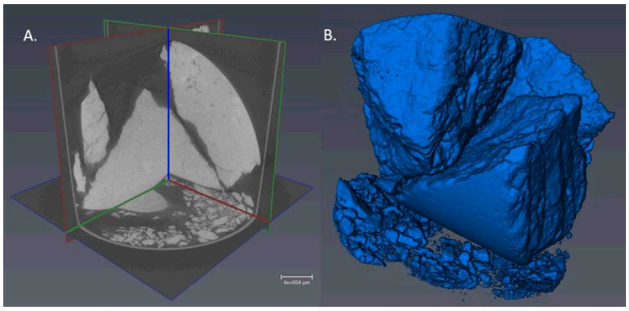

Figure 5. X-ray tomographic reconstruction of “dropped” DRZ core piece.

4.4 Grain Size Distributions of "run of mine" salt floor samples

A preliminary estimation of the grain size distribution of the run-of-mine salt bucket was determined using the Pergeos software, using a small subset of the bucket one decimeter in volume taken from the middle bottom portion of the bucket shown in Figure 4 which is depicted in Figure 6. The image on the left side show the original grey-level reconstruction from the tiff stack, the image in the middle shows segmented grains, shown in blue, and the right image shows grain separates using a proprietary watershed algorithm for separating grains. The grain separates are shown in different colors. A close inspection shows that several of the larger grains have been separated into two or more smaller grains, but that most of the smaller equant grains have been recognized and separated successfully. It is likely that the Pergeos watershed algorithm works best for equant grains, such as occurs in a well sorted sandstone, and that the larger, pancake-shaped grains are not well separated by the software.

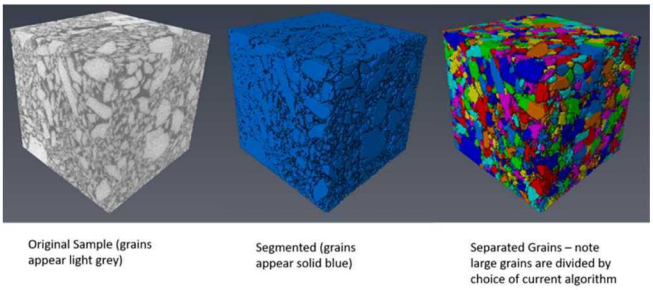

Figure 6. Decimeter volume of run-of-mine salt bucket, showing original grey levels (left), segmented solid phase (middle), and separated grains (right).

The resulting grain size distribution is shown via a frequency histogram in Figure 7, with particle size shown as a phi-scale (log-base 2) of grains in mm. A bi-modal distribution is evident, and we suggest that most of the more frequent smaller grains below ~ 1mm in size (a phi value of ~ 0.0) can safely be deleted from consideration due to negligible volumes (this is the grain sizes expressed by the blue box; the extreme left side of the distribution with the smallest sizes plotted in Figure 7 are essentially equivalent to just a few voxel sizes, and thus are not well resolved in the image set). In Figure 7, 43,850 grains were recognized, with 3414 grains existing in the greater-than-1 mm size fraction.

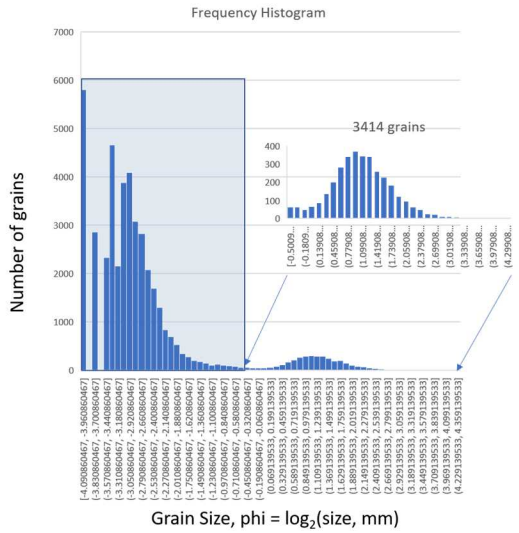

Figure 7. Frequency histogram of grain separates in Figure 6, with grain size expressed in phi scale (log base 2 of grain size in mm).

4.5 Grain Separates

As a proof of concept, we constructed surface meshes in STL format of grain separates, and show how these files can be used in simulations of room rubble consolidation. The Scan-IP software watershed algorithm was used in a similar fashion to the Pergeos method, and the grain separates are shown in different colors in Figure 8. An STL surface mesh was made form the teal-colored grain, which is discussed in the next section.

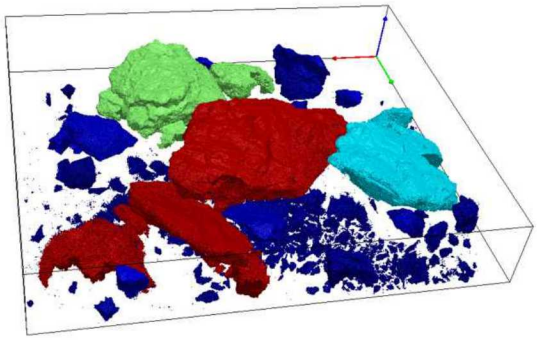

Figure 8. Grain separates taken from the top of the run-of-mine salt shown in Figures 3 and 4 (for relative scale reference, the center most red grain is 5mm along is long axis)).

4.6 Cyberstone™ Modeling

The Geocosm portion of this project involves simulating the deposition and mechanical compaction of rubble that forms in association with clasts that fall from the ceilings of collapsing chambers at the WIPP site. The deposition portion of this work uses rigid-body physics simulations that consider complex 3D shapes for clasts as they collide with the chamber floor and one another. The mechanical compaction phase of the work will use these simulated rubble deposits as starting points for simulations that consider clast deformation response to imposed stresses.

Our efforts thus far in the project have focused on proof-of-concept simulations of rubble deposition. The tasks involved include (1) preparing the 3D geometry for an example salt clast from the WIPP site for collision detection (previous section) and (2) simulating a rubble deposit using this clast using Geocosm's Cyberstone system. In conducting this analysis, we demonstrated that the data types, workflows, and simulation codes for rubble deposition all are functioning optimally. The simulation result that we describe below, however, is not intended to be representative of rubble deposits that are likely to occur at the WIPP site, which will be based on full size distributions prepared from the rubble.

The first portion of our analysis was to pre-process the 3D geometry for a clast from the WIPP site for rigid body physics simulation. Accurate collision detection for irregular, non-convex clasts is an extremely complex endeavor. Collision detection for objects with convex surfaces, by contrast, is computationally far simpler. Consequently, we use the hierarchical approximate convex decomposition approach (Mamou, 2010) to represent each individual clast as a connected set of convex surface meshes. The result of this analysis on the example clast from the WIPP site is shown in Figures 9 and 10 where the clast geometry is indicated in blue and the convex meshes that approximate it are shown in red. For the most part the convex decomposition process results in a geometry that closely mimics the actual grain shape. The most notable deviations in shape are indicated by the green arrows in the figures. Our assessment of this result is (1) that such deviations are likely to be less common for clasts shapes that omit neighboring clasts and (2) even for this example the impact of this deviation on simulated rubble packing geometries is likely negligible.

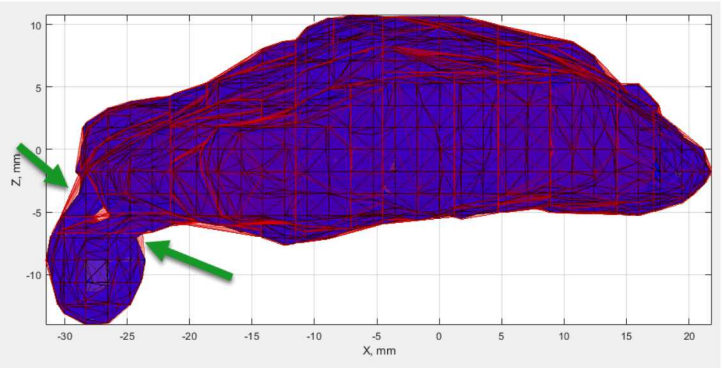

Figure 9. An example salt clast geometry from the WIPP site in blue together with the convex meshes that approximate it in red. The green arrows indicate regions where the convex meshes deviate somewhat from the clast shape.

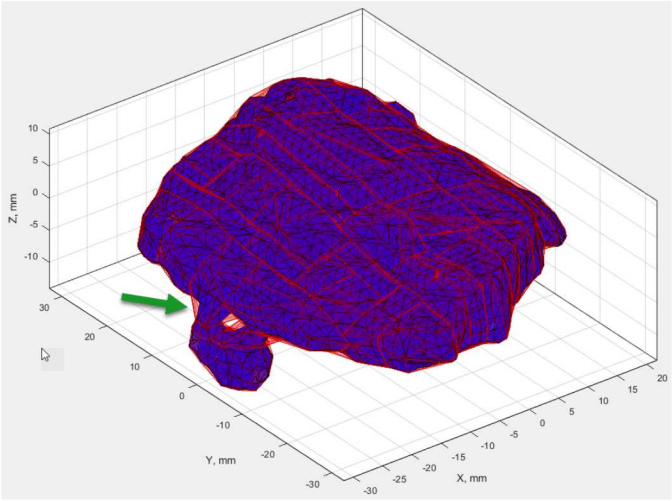

Figure 10. An alternative perspective of the same clast (blue) and convex meshes (red) shown in Figure 10.

In the second portion of our proof-of-concept analysis we used the clast depicted in Figures 9 and 10 as input for a simple rubble deposition simulation. In the simulation we arbitrarily allow the clasts that are deposited to have long axis lengths that range from 3.2 to 6.4 cm. In the simulation 1750 clasts were given random orientations and then dropped at random locations within a cylindrical container with a diameter of 40 cm (Figure 11).

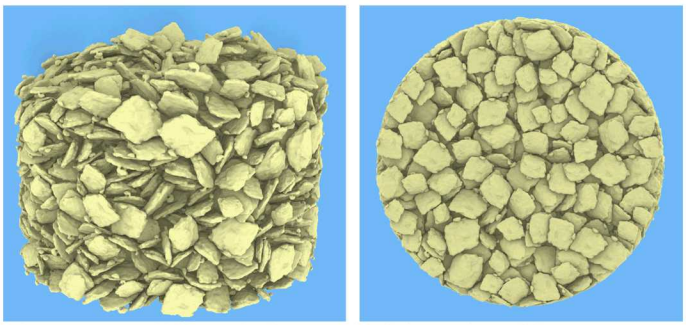
Figure 11. Rubble pack that resulted from depositing 1750 clasts with the shape shown in Figure 9 into a cylindrical container.

The flake-like shape of the reference clast results in cases where clasts in the deposition simulation obtain vertical orientations adjacent to the container walls. Consequently, to get a more realistic depiction of the internal structure of the rubble pack it is necessary to trim away the outer portions of the simulated pack as indicated in Figure 12. Here we see the tendency for the clast particles to have sub-horizontal orientations. The porosity for this simulation is likely significantly higher compared to rubble that occurs at the WIPP site for several reasons: (1) the variation in clast sizes is much lower than expected at the WIPP site, (2) most of the clasts at the WIPP site have more equant forms (particularly in the finer size fractions) and (3) the irregular bump on the clast associated with the smaller unresolved neighboring clast (see Figures 1 and 2) reduces the packing efficiency and increases the effective friction.

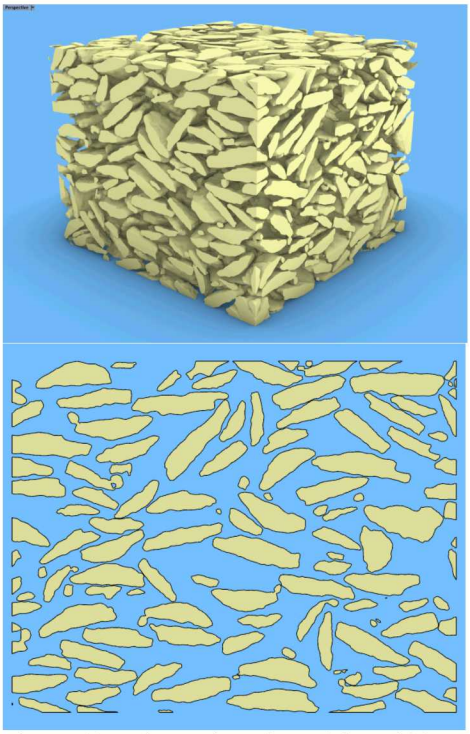
Figure 12. Trimmed portion of the rubble pack shown in Figure 11. Top: 3D geometry of trimmed region. Bottom: a vertical cross section along the pack x-axis.

4.7 CFD Modeling of Gas Transport in DRZ Core Fractures

To demonstrate how gas flux through the consolidating rubble pile can be simulated to estimate permeability and other transport properties, we first show connected volumes in the DRZ core piece in Figure 13. The en echelon shapes of the extension fractures are evident in the segmented volumes of the fractures. We applied a flood-fill algorithm in the Scan-IP software to several of the larger fracture volumes, and the results shown that the fractures are percolating along the axis of the fractures, but are not connected to fractures above and below at least in the segmented volume examined, in that each color represents a unique connected volume.

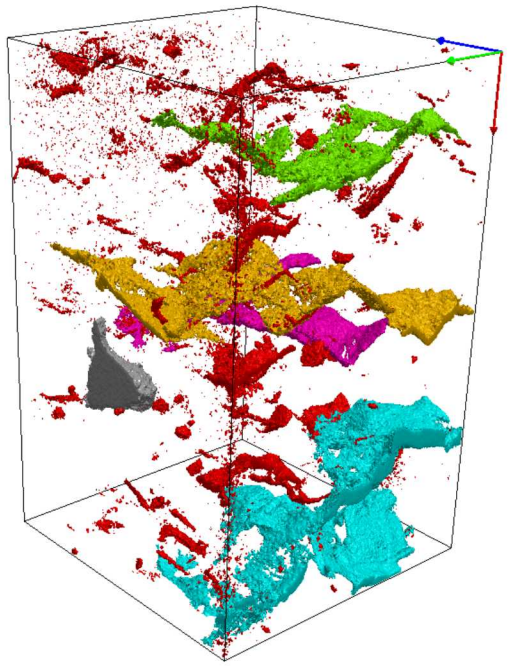

Figure 13. Connected volumes shown in different colors, for the extension fractures in the DRZ core piece shown in Figure 2A. For scale reference, the vertical access in Fig. 13 is on the order of 10 inches (250mm).

We selected the "gold" colored fracture volume and used the Scan-FE algorithm to obtain a CFD triangular mesh for simulation purposes, shown in Figure 14. An example simulation of dry air transport is shown in Figure 15.

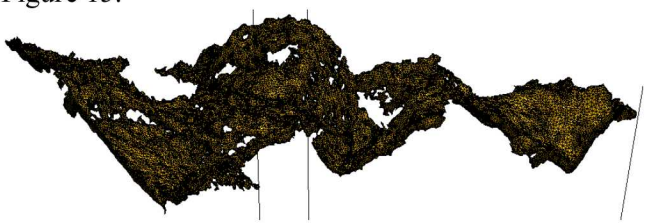

Figure 14. Triangular CFD mesh of WIPP DRZ core piece fracture (the fracture is on the order of 100mm).

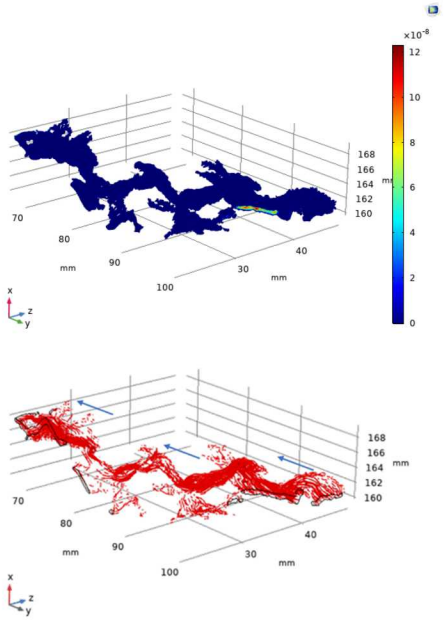

Figure 15. Flow simulations of dry air transport through DRZ fracture using mesh shown in Figure 14 with COMSOL Multiphysics. The left figure shows velocity (although not evident in the image, the interior of the volume shows velocities of 1.0e-8 m/s for the boundary conditions chosen. The right figure shows simulated stream lines, depicting a central flow pathway and several "dead-end" portions of the fracture volume.

5. CONCLUSIONS

We demonstrate a workflow for examining roof-fall consolidation and evolution of transport properties in the consolidating mass. This involves:

1. Characterization of rubble size and shape using X-ray micro-computed tomography
2. Image analysis to include solid segmentation and grain separation, using a variety of filters and watershed methods.
3. Creation of grain size distributions of rubble piles
4. Creation of grain surface meshes extracted from the separated particles, using the distribution as a guide.
5. Cyberstone modeling of rubble consolidation, extracting representative shapes and sizes using the provided STL files and the resulting volume distribution as a guide.
6. CFD modeling of gas transport in the consolidating rubble piles from the Cyberstone results.

One earlier conclusion is that it appears that the DRZ fractures percolate along the fracture lengths through centralized flow pathways but appear to not interact with nearby fractures. Current work involves perfecting the grain separation methods using different image analysis techniques and software. This will refine

the distributions and grain mesh files passed to Geocosm for the consolidation simulations.

REFERENCES

1. Carrasco, R. (Sept. 2019b). *Roof fall photographs*. Personal Communication.
2. Mamou, K., 2010, Approximate Convex Decomposition for Real-Time Collision Detection, Game Programming Gems 8 (March 2010).

ACKNOWLEDGMENTS

Sandia National Laboratories is a multi-mission laboratory managed and operated by National Technology and Engineering Solutions of Sandia LLC, a wholly-owned subsidiary of Honeywell International Inc. for the U.S. Department of Energy's National Nuclear Security Administration under contract DE-NA0003525.
This research is funded by WIPP programs administered by the Office of Environmental Management (EM) of the U.S. Department of Energy. SAND2020-xxxx C.